Bipyridinium Macroring Encapsulated within Zeolite Y Supercages. Preparation and Intrazeolitic Photochemistry of a Common Electron Acceptor Component of Rotaxanes and Catenanes§

Mercedes Alvaro,† Belén Ferrer,† Vicente Fornés,† Hermenegildo García,*,† and J. C. Scaiano*,‡

Instituto de Tecnología Química CSIC−UPV and Departamento de Química, Universidad Politécnica de Valencia, Avda. de los Naranjos s/n, 46022 Valencia, Spain, and Department of Chemistry, Centre for Catalysis Research and Innovation, University of Ottawa, 10 Marie Curie, Ottawa K1G 6N5, Canada

Received: November 8, 2001; In Final Form: February 11, 2002

Cyclobis-(N,N′-paraquat-*p*-phenylene) macrocycle ($\mathbf{2}^{4+}$), the electron acceptor ring present in many [2]-catenanes and rotaxanes, has been obtained encapsulated within the supercages of zeolite Y by ship-in-a-bottle synthesis from the open precursor ($\mathbf{1}^{2+}$) and 1,4-bis(bromomethyl)benzene. Upon 266 nm laser excitation, the corresponding $\mathbf{1}^{\bullet+}$ and $\mathbf{2}^{\bullet(3+)}$ radical cations living hundreds of μs are generated within the zeolite cages in line with the photochemical behavior reported for the parent methyl viologen included within zeolites. Addition of 1,4-dimethoxybenzene (**DMB**) to $\mathbf{1}^{2+}$@Y and $\mathbf{2}^{4+}$@Y leads to the formation of the corresponding charge transfer (CT) complexes characterized by a broad CT band at λ_{max} 475 nm. Laser flash photolysis at 266 nm of $\mathbf{1}^{2+}$@Y and $\mathbf{2}^{4+}$@Y containing **DMB** shows a dramatic reduction of the signal of the $\mathbf{1}^{\bullet+}$ and $\mathbf{2}^{\bullet(3+)}$ radical cations due to the electron-transfer quenching of $\mathbf{1}^{2+}$ and $\mathbf{2}^{4+}$ excited states by **DMB**. In contrast, 532 nm selective excitation of the $\mathbf{1}^{2+}$**-DMB** or $\mathbf{2}^{4+}$**-DMB** CT complexes allowed the detection of $\mathbf{1}^{\bullet+}$ and $\mathbf{2}^{\bullet(3+)}$ radical cations and $(\mathbf{DMB})_2^{\bullet+}$ as long-lived transients whose decay was not complete after hundreds of microseconds following laser excitation. Generation of $(\mathbf{DMB})_2^{\bullet+}$ upon excitation of the $\mathbf{2}^{4+}$**-DMB** CT complex indicates that the initially complexed $\mathbf{DMB}^{\bullet+}$ migrates out of the macroring and becomes stabilized by interaction with an electron-rich neutral **DMB** molecule, forming a dimer. This photochemical behavior is distinctive of restricted media because no transients are detected in the nanosecond time scale-upon 355 or 532 nm laser photolysis of the same $\mathbf{1}^{2+}$**-DMB** or $\mathbf{2}^{4+}$**-DMB** CT complexes in acetonitrile. Our results illustrate the potential of zeolites in the field of molecular machines as a medium to stabilize short-lived transients.

Introduction

Recent years have witnessed an impressive research effort aimed at the preparation, characterization, and study of the properties of rotaxanes and catenanes.[1,2] The outcome of this research has led to the development of smart molecules, molecular machinery, and devices for data storage at the molecular level. Many of these supramolecular assemblies are synthesized using charge transfer (CT) complexation between a donor and an acceptor moiety as the structure-directing interaction. In this strategy, the most commonly employed acceptor moiety is the cyclobis-(N,N′-paraquat-*p*-phenylene) macrocycle. This electron-poor macroring can be prepared by cyclization of a precursor having two 4,4-bipyridine units attached at the para position of a phenylene moiety ($\mathbf{1}^{2+}$) with 1,4-bis(bromomethyl)benzene (Scheme 1).[3]

As a part of a project directed to the encapsulation of rotaxanes and catenanes within the rigid internal voids of zeolites and related porous silicates,[4] we describe here the *ship-in-a-bottle* synthesis of cyclophane $\mathbf{2}^{4+}$. We provide a comparative study of the photochemical properties of $\mathbf{2}^{4+}$ within zeolite Y and in solution. To provide a more complete description of the differences in the photoresponse of the macroring $\mathbf{2}^{4+}$ upon inclusion in the supercages of Y zeolite, the corresponding uncyclized precursor $\mathbf{1}^{2+}$ is also included in this study.

SCHEME 1

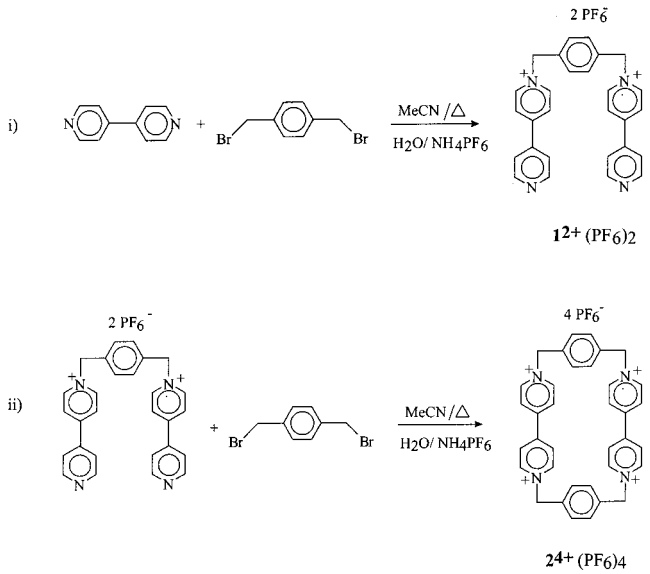

Results and Discussion

On the basis of the reported single-crystal X-ray diffraction of compound $\mathbf{2}^{4+}$ and a [2]-catenane comprising $\mathbf{2}^{4+}$ as electron-

† Instituto de Tecnología Química CSIC−UPV and Departamento de Química, Universidad Politécnica de Valencia.

‡ Department of Chemistry, Centre for Catalysis Research and Innovation, University of Ottawa.

§ Dedicated to Professor Waldemar Adam as he approaches a new landmark.

10.1021/jp014088u CCC: $22.00
Published on Web 06/07/2002

SCHEME 2

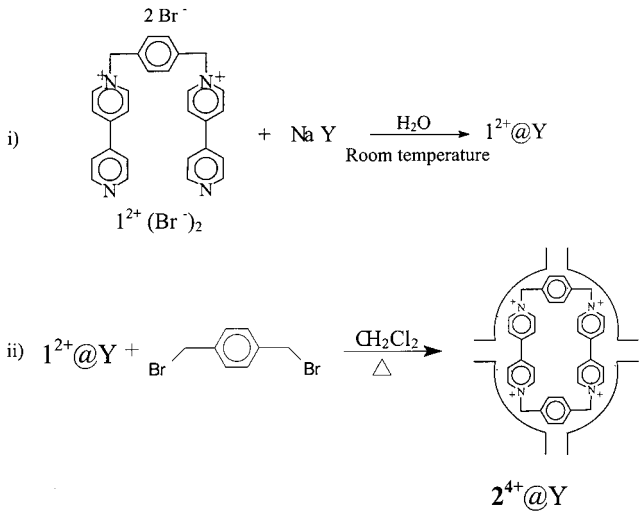

acceptor unit,[3] the dimension of $\mathbf{2}^{4+}$ (7.4 × 10.3 Å) is too large to allow its free diffusion from the exterior to the interior of the zeolite particles through the round 12 member ring opening of zeolite Y supercages (∼7 Å diameter). For tridirectional, large-pore zeolites such as zeolite Y, one can envision a situation in which even though a guest is too big to enter through the smaller pore apertures, it could fit inside the much larger cavities. This is the case of compound $\mathbf{2}^{4+}$, whose reported molecular size is sufficiently small to be accommodated inside the spherical supercages of zeolite Y (∼13 Å diameter). A useful strategy for this situation is termed *ship-in-a-bottle* synthesis, and consists of constructing the molecule by reacting smaller precursors within the cavity.[5,6] Because chromatographic purification is not possible after the *ship-in-a-bottle* synthesis, the reactions employed have to be highly selective, or the byproducts must be small enough to fit through the cavity windows, so that they can be removed by solid−liquid extraction. The simplest approach is to emulate the synthetic route that has been demonstrated to work in homogeneous phase.[7]

In our case, we have adapted the reported synthetic preparation to obtain $\mathbf{2}^{4+}$ by *ship-in-a-bottle* synthesis (Scheme 2). Because the open precursor $\mathbf{1}^{2+}$ has conformational flexibility with a molecular kinetic diameter close to that of benzene, it is anticipated that it can be incorporated easily inside the cavities. Thus, we started from the commercially available Na^+-form of the Y zeolite and proceeded to ion exchange Na^+ by $\mathbf{1}^{2+}$ from an aqueous solution. The success of the exchange can be assessed from the disappearance of $\mathbf{1}^{2+}$ in the aqueous solution. The estimated loading determined by combustion chemical analysis of the solid was one molecule of $\mathbf{1}^{2+}$per 8 zeolite supercages.

Formation of $\mathbf{2}^{4+}$ encapsulated within the cages of Y zeolite was accomplished by treating $\mathbf{1}^{2+}$@Y with 1,4-bis-(bromomethyl)benzene in dichloromethane at reflux temperature for 3 d. A slight excess of the phenylene reagent was added to overcome the possible consumption of this reagent by reaction with coadsorbed water or silanol groups present in the zeolite.

Concerning the influence of the confinement inside the zeolite supercage on the formation of $\mathbf{2}^{4+}$ by cyclization, it was anticipated that the zeolite framework will exert some templating effect favoring the ring closure versus linear or cyclic oligomerization. Shape selectivity in product formation is well documented in catalysis by zeolites.[8,9] This effect describes the fact that the main factor controlling product formation in zeolites

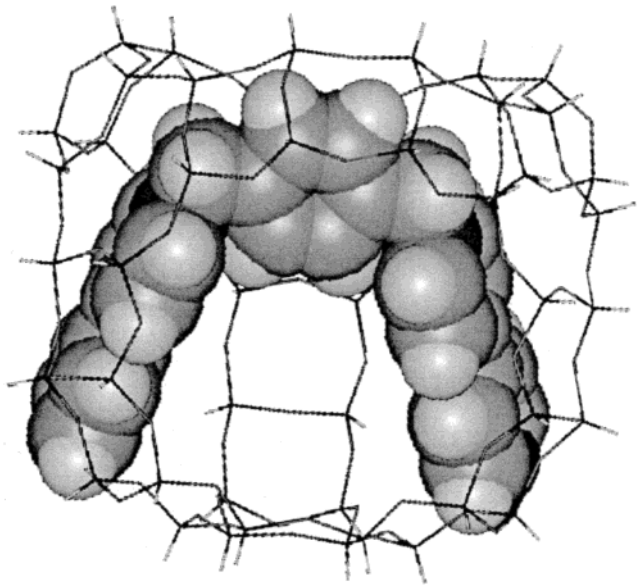

Figure 1. Molecular modeling of the compound $\mathbf{1}^{2+}$ inside the supercage of zeolite Y.

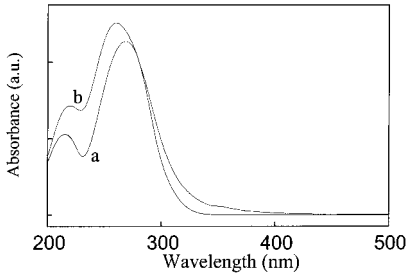

Figure 2. Diffuse reflectance UV−vis spectra (plotted as the inverse of the reflectance, R) of cations $\mathbf{1}^{2+}$ (a) and $\mathbf{2}^{4+}$ (b) encapsulated within the cavities of Y zeolite.

can be the molecular shape, the predominant product being the one that better fits inside the zeolite micropores. This templating effect derives from the fact that each supercavity of NaY contains four exchangeable Na^+ ions that are replaced by the positive charges of $\mathbf{1}^{2+}$. Molecular modeling at molecular dynamics level shows that given the distance between the positive charges in $\mathbf{1}^{2+}$, the only possibility is that the two positive N of $\mathbf{1}^{2+}$ share the same cavity and this forces a proximity between the two terminal pyridyl units. A visualization of the molecular model is shown in Figure 1. Precedents about the influence of the encapsulation inside zeolite cavities promoting macrocyclization versus oligomerization can be found in the literature [10]

The success of the cyclization and formation of the bipyridinium macroring $\mathbf{2}^{4+}$ was firmly assessed by comparing the spectra of the sample $\mathbf{2}^{4+}$@Y with those of an authentic sample of $\mathbf{2}^{4+}(\mathbf{PF_6})_4$ and its precursor $\mathbf{1}^{2+}$@Y. Figures 2-4 shows the diffuse reflectance UV spectra, the solid-state MAS ^{13}C NMR and the FT-IR of samples $\mathbf{1}^{2+}$@Y and $\mathbf{2}^{4+}$@Y. As anticipated based on the known spectra of $\mathbf{1}^{2+}$ and $\mathbf{2}^{4+}$ in solution,[3] the optical and the ^{13}C NMR spectra of samples $\mathbf{1}^{2+}$@Y and $\mathbf{2}^{4+}$@Y were almost indistinguishable and did not allow to determine whether the macroring cyclization leading to $\mathbf{2}^{4+}$ has occurred and what is the purity of the encapsulated material. Particularly, solid-state ^{13}C NMR spectroscopy (Figure 3), although it clearly shows the presence of pyridinium units, it does not have sufficient resolution to distinguish between adsorbed $\mathbf{1}^{2+}$ and $\mathbf{2}^{4+}$. In this regard, IR spectroscopy was more informative.

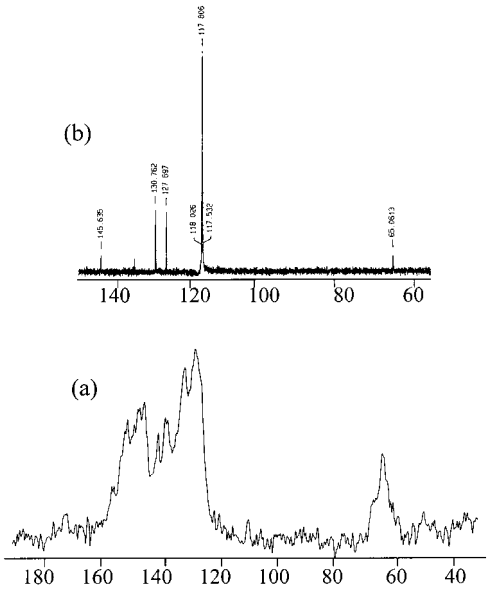

Figure 3. Solid-state MAS ^{13}C NMR of the $\mathbf{2}^{4+}$@Y sample (a) and ^{13}C NMR of the $\mathbf{2(PF_6)_4}$ in CD_3CN (b).

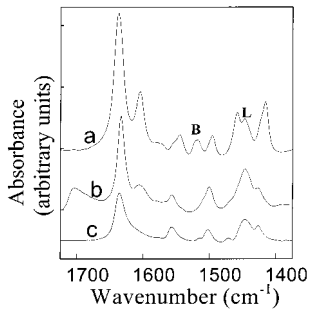

Figure 4. Aromatic region of the FT-IR spectra of $\mathbf{1}^{2+}$@Y (a) and $\mathbf{2}^{4+}$@Y (b) recorded at room temperature after outgassing the samples at 200 °C for 1 h at 10^{-2} Pa. Spectrum c corresponds to an authentic sample of $\mathbf{2}^{4+}$ $(PF_6)_4$ in KBr disk. The peak labeled as B corresponds to pyridine interacting with Bronsted sites and is observed for $\mathbf{1}^{2+}$@Y. The peak labeled as L corresponds to *N*-alkylpyridinium and is present in the IR spectra of $\mathbf{1}^{2+}$@Y, $\mathbf{2}^{4+}$@Y and $\mathbf{2}^{4+}$ $(PF_6)_4$.

The IR spectra of pyridine, pyridinium, and N-alkyl substituted pyridinium ions incorporated in many types of zeolites has been subject to intensive studies.[11] Pyridine is the most widely used base to titrate solid acids because it shows distinctive and reliable aromatic vibration bands depending on the status of the aromatic N atom. These specific bands of pyridine in the aromatic region are known to be safe identification criterion that has been used in a considerable number of reports.[11−14] Thus, pyridinium ions formed by protonation of basic pyridine on zeolite Brønsted centers has a characteristic band at 1540 cm^{-1} (labeled B in Figure 4), while Lewis pyridine adducts and N-alkyl pyridinium exhibit a peak at 1450 cm^{-1} (labeled L in Figure 4). As shown in Figure 4, authentic compound $\mathbf{1}^{2+}$included in the zeolite by ion exchange contains both bands corresponding to *N*-alkylpyridinium and free pyridine ring. In contrast, after further alkylation (Scheme 2), the IR spectrum becomes simpler due to the symmetry of compound $\mathbf{2}^{4+}$, and the only vibration bands observed are those corresponding to *N*-alkylpyridinium (labeled as L in Figure 4), whereas hydrogen-pyridinium peak (labeled as B in Figure 4) has disappeared in the IR spectrum of $\mathbf{2}^{4+}$@Y and $\mathbf{2}^{4+}\mathbf{(PF_6)_4}$. Furthermore, the aromatic region of the IR spectrum of $\mathbf{2}^{4+}$@Y taken as a fingerprint resembles closely that recorded for the $\mathbf{2}^{4+}$ $(PF_6)_4$ salt in KBr disk. This good match was considered also an indication to assess the purity of $\mathbf{2}^{4+}$ inside the zeolite, since the only extra IR band was a weak band due to C═O group. This C═O could indicate the presence of residual amounts of an aromatic aldehyde formed by intrazeolite oxidation of 1,4-bis-(bromomethyl)benzene or hydroxyderivative. A control carried out under the same conditions in the absence of $\mathbf{1}^{2+}$ reveals that 1,4-bis-(bromomethyl)benzene undergoes a small degree of oxidation upon contacting with dehydrated zeolite.

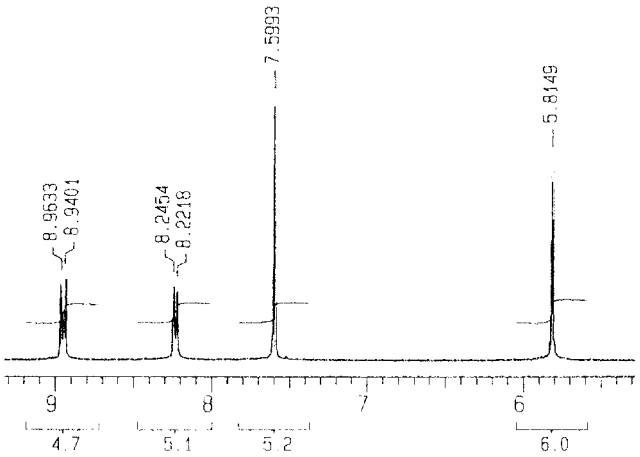

Figure 5. ^1H NMR of the compound $\mathbf{2}^{4+}$ after dissolving the zeolite framework.

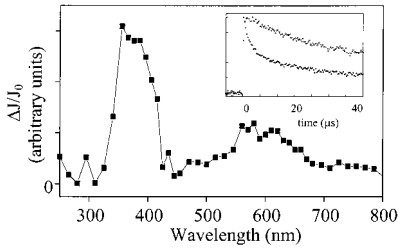

Figure 6. Transient diffuse reflectance UV−vis spectra of a N_2-purged $\mathbf{1}^{2+}$@Y sample recorded 2 μs after 266 nm laser pulse. The inset shows normalized decays monitored at 385 (△) and 600 nm (○).

Alternatively, formation of $\mathbf{2}^{4+}$ was unambiguously demonstrated by dissolving the zeolite framework with HF acid under mild conditions. Solid−liquid extraction of the resulting solid residue after neutralization allowed detecting compound $\mathbf{2}^{4+}$ by conventional liquid ^1H NMR in D_2O. Figure 5 shows the ^1H NMR spectrum of the basified aqueous liquor after dissolving the zeolite.

Laser Flash Photolysis of $\mathbf{1}^{2+}$@Y, $\mathbf{2}^{4+}$@Y and their DMB CT Complexes. Samples of $\mathbf{1}^{2+}$@Y and $\mathbf{2}^{4+}$@Y were submitted to diffuse reflectance laser flash photolysis. As expected, on the basis of related reports on the photochemistry of methyl viologen (MV^{2+}) in Y zeolites,[15−18] 266 nm laser excitation leads to the observation of the corresponding radical cations (Figures 6 and 7).

In the case of $\mathbf{2}^{4+}$@Y the transient spectrum is very similar to that reported for MV^{2+} in solution or zeolite,[18] characterized by a sharper, more intense absorption peak at 390 nm and a much broader, less-intense band with fine structure at around 600 nm. Decays monitored at 400 and 640 nm are compatible with the presence of a single species. In the case of $\mathbf{1}^{2+}$@Y, the spectrum was similar, but the band at 390 nm was broader and contains a shorter component that is quenched by oxygen. On the basis of the similarity with biphenyl, we assigned this shorter-lived transient absorbing at λ_{max} 370 nm to $\mathbf{1}^{2+}$ triplet excited state. The same spectra (albeit much less intense) and

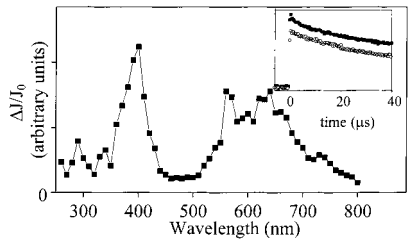

Figure 7. Transient diffuse reflectance UV−vis spectra of a N_2-purged $\mathbf{2}^{4+}$@Y sample recorded 2 μs after 266 nm laser pulse. The inset shows the signal decays monitored at 400 (■) and 640 nm (○).

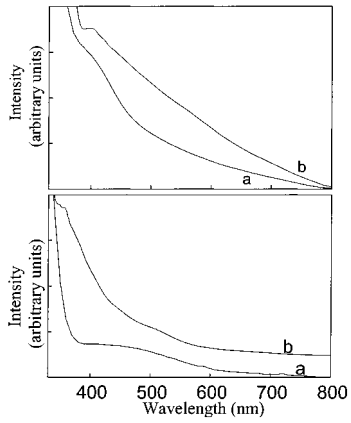

Figure 8. UV−vis spectra of $\mathbf{1}^{2+}$**/DMB** complex (top) and $\mathbf{2}^{4+}$**/DMB** complex (bottom) in CH_3CN (a, Absorbance) and included inside zeolite NaY (b, diffuse reflectance plotted as 1/R).

lifetimes are obtained using 355 nm laser excitation, probably due to some residual absorption of $\mathbf{1}^{2+}$ and $\mathbf{2}^{4+}$ as consequence of the broadening of the absorption band upon inclusion in zeolite.[18,19] However, using 532 nm laser excitation, virtually no signal was observed. This result will become relevant when commenting the laser flash photolysis spectra of the CT complexes of $\mathbf{1}^{2+}$ and $\mathbf{2}^{4+}$ with **DMB** encapsulated within zeolite Y.

Importantly, control experiments working with $\mathbf{1}^{2+}$ and $\mathbf{2}^{4+}$ in dry acetonitrile solutions did not reveal any detectable transient. This is consistent with the behavior of the parent MV^{2+} in solution and with the lack of a suitable electron donor in dry solutions.[20]

As mentioned in the Introduction, the most relevant current application of the macroring $\mathbf{2}^{4+}$ is as electron-acceptor component in catenanes and rotaxanes.[1,21] The assembly and specific features of other CT complexes incorporated in zeolites are well documented.[16,19,22−24] Methyl viologen has been the most widely used, electron acceptor moiety for these studies.[16] Therefore, in view of these precedents it was anticipated that both $\mathbf{1}^{2+}$@Y and $\mathbf{2}^{4+}$@Y samples could easily form CT complexes with electron-rich aromatic molecules such as **DMB**, as it turned out to be the case.

Upon adsorption of an excess of **DMB** from a dichloromethane solution onto the $\mathbf{1}^{2+}$@Y and $\mathbf{2}^{4+}$@Y samples, the color of the zeolites changes from white to gray and the corresponding diffuse reflectance of the solids shows a change in the baseline. Figure 8 compares the optical spectrum of $\mathbf{1}^{2+}$ and $\mathbf{2}^{4+}$ in the presence of **DMB** in solution and in zeolite. The drift in the baseline observed in the diffuse reflectance spectra of $\mathbf{1}^{2+}$**-DMB** and $\mathbf{2}^{4+}$**-DMB** in zeolite Y could indicate that a CT complex is formed inside the zeolite. None of the two components of the complex has absorption at such long-wavelength and per se can explain the drift of the baseline observed in the optical spectra.

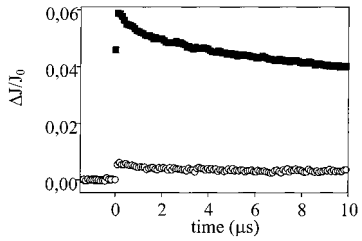

Figure 9. Comparison of the transient decays upon 266 nm laser excitation monitored at 600 nm for the $\mathbf{2}^{4+}$@Y sample prior (■) and after (○) addition of **DMB**. The samples were purged with N_2 and were recorded inmediatly one after the other under the same experimental conditions.

Laser flash photolysis of encapsulated $\mathbf{1}^{2+}$**-DMB** and $\mathbf{2}^{4+}$**-DMB** CT complexes was carried out using 266 and 532 nm laser excitation. In the experiments using 266 nm, simultaneous excitation of uncomplexed $\mathbf{1}^{2+}$ or $\mathbf{2}^{4+}$ as well as **DMB** and the CT complex can occur. Although it is obvious that 266 nm wavelength does not allow selective excitation of the CT complex, we wanted to have an estimation of the behavior of uncomplexed $\mathbf{1}^{2+}$ and $\mathbf{2}^{4+}$ under comparable conditions as those used to record Figures 6 and 7. Essentially the same spectra as those shown in Figures 6 and 7 were recorded even in the presence of **DMB,** although an enormous reduction in the intensity of the signal was observed. Figure 9 provides a comparison of the signals obtained for $\mathbf{2}^{4+}$ in the presence and absence of **DMB** under otherwise the same conditions and laser power. This dramatic decrease in the intensity of the signal is consistent with the electron-transfer quenching of $\mathbf{1}^{2+}$ or $\mathbf{2}^{4+}$ excited states by **DMB**, followed by fast back electron transfer. This provides an efficient energy waste pathway of $\mathbf{1}^{2+}$ or $\mathbf{2}^{4+}$ excited states. These rapid processes are known to occur in solution in the subnanosecond time scale.[25] Because the system can be considered static, only the residual, minor population of $\mathbf{1}^{2+}$ or $\mathbf{2}^{4+}$ molecules that do not have **DMB** in sufficiently close proximity to be quenched do still generate the corresponding radical cation. These unquenched molecules are the transients that can be detected in the time scale available for our diffuse reflectance nanosecond setup.

In contrast, totally different results were obtained upon 532 nm laser excitation. Using this laser no excitation of uncomplexed $\mathbf{1}^{2+}$ or $\mathbf{2}^{4+}$ occurs (vide supra). Therefore, this laser wavelength exclusively probes the photochemistry of encapsulated $\mathbf{1}^{2+}$**-DMB** and $\mathbf{2}^{4+}$**-DMB** assemblies. In a seminal work dealing with the stability of radical ions within zeolites, Kochi and co-workers demonstrated that the lifetime of contact ion pairs generated photochemically upon excitation of MV^{2+} and electron-rich aromatic compounds CT complexes in zeolite is in the microsecond time scale. This is 10^6-fold longer-lived that the same species in solution.[15] We anticipated that the same behavior should be observed for the $\mathbf{1}^{2+}$@Y and $\mathbf{2}^{4+}$@Y containing **DMB** as electron donor.

Figures 10 and 11 provide a comparison of the transient spectra upon 532 nm excitation of the samples $\mathbf{1}^{2+}$@Y and $\mathbf{2}^{4+}$@Y before and after addition of **DMB**. The bands at ∼390 and ∼600 nm must correspond to the radical cations of $\mathbf{1}^{\bullet+}$ and $\mathbf{2}^{\bullet(3+)}$ as in spectra of Figures 6 and 7. However, no band attributable to $\mathbf{DMB}^{\bullet+}$ that has reported to appear at 430 nm was observed.[26] In contrast, an intense absorption band was recorded at $\lambda_{max} \approx 800$ nm. We attribute this band to $(\mathbf{DMB})_2^{\bullet+}$ dimer radical cation based on related reports on the behavior of benzene, anisole,[27−30] phenylsulfides, aniline, and amines radical cations that all form the corresponding dimer radical cation. To support the assignment of the ∼800 nm band to

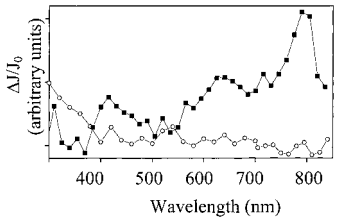

Figure 10. Comparison of the transient diffuse reflectance UV−vis spectra of N_2-purged $\mathbf{1}^{2+}$@Y samples prior (○) and after (■) addition of **DMB** recorded 2 μs after 532 nm laser pulse.

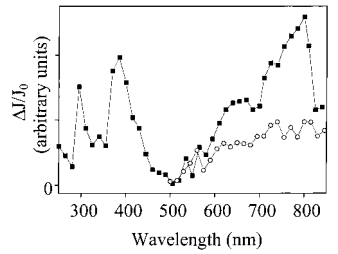

Figure 11. Comparison of the transient diffuse reflectance UV−vis spectra of N_2-purged $\mathbf{2}^{4+}$@Y samples prior (○) and after (■) addition of **DMB** recorded 2 μs after 532 nm laser pulse.

SCHEME 3

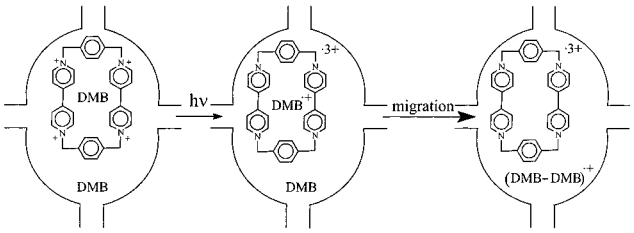

$(\mathbf{DMB})_2^{\bullet+}$ dimer radical cation, laser flash photolysis of a different sample of viologen anchored on aluminosilicates containing **DMB**[31] was carried out allowing to record the same transient.

Formation of $\mathbf{1}^{\bullet+}$ or $\mathbf{2}^{\bullet(3+)}$ as well as $(\mathbf{DMB})_2^{\bullet+}$ can be rationalized assuming that upon selective excitation of the $\mathbf{1}^{2+}$-**DMB** and $\mathbf{2}^{4+}$-**DMB** CT complexes inside the zeolite Y supercage prompt electron transfer occurs (Scheme 3). Repulsive electrostatic interactions promote migration of the primary $\mathbf{DMB}^{\bullet+}$ radical cation from the initial CT complex out of the cyclophane macroring and will become stabilized by interaction with a second **DMB**. All of the processes must be complete within the 15−20 ns time resolution of our diffuse reflectance setup because no growth of the signal at 800 nm has been recorded. Of the processes shown in Scheme 3, the migration of **DMB** must be the slowest one. The fact that some excess of **DMB** must be present in the zeolite (average loading 1.5 per supercage) to form the CT complex contributes to favor the formation of $(\mathbf{DMB})_2^{\bullet+}$ and the proximity between the CT complexes and free **DMB** should make it sufficiently rapid to become instantaneous in our time scale. In this regard, by using a picosecond laser system, we have previously measured that excimer (a dimer of a ground and an excited state) formation between pyrenes occupying the same supercage of a zeolite Y is complete in the first 15 ns after the laser pulse.[32]

Importantly, our own 355 or 532 nm laser flash of $\mathbf{1}^{2+}$-**DMB** and $\mathbf{2}^{4+}$-**DMB** CT complexes in acetonitrile solution did not lead to the detection of any transient in the available time scale.[25] In view of the studies of related CT complexes of $\mathbf{2}^{4+}$ and MV^{2+} with aromatic donors, the most likely explanation is that in solution back electron transfer of photogenerated radical ions is very fast and efficient, leading to the complete annihilation of the transients in a few hundreds of ps.[25] Therefore, the distinctive photochemical behavior of the $\mathbf{1}^{2+}$-**DMB** and $\mathbf{2}^{4+}$-**DMB** CT complexes included within Y zeolite will be again a reflection of the ability of this solid matrix to increase the lifetime of elusive radical cations. Concerning the origin of the remarkable long lifetime of the charge separated state of the CT complex, besides polarity effects previously invoked,[15] we suggest that the possibility of random walk of the electron through the zeolite framework should also be considered. Indeed, the active participation of the zeolite framework as electron donor or acceptor in photoinduced electron transfer of adsorbed organic guests is well documented.[7] In other words, even if the CT complex is selectively excited, the hole or the electron could be transferred to the zeolite framework, giving rise to the detection of the same transients but not as a partners but in different complexes.

In summary, given that the cyclophane $\mathbf{2}^{4+}$ is a common component of many catenanes and rotaxanes, the present report opens the way to prepare these supramolecular systems within the pores of tridirectional, large pore zeolites. The anticipated advantages of this strategy will be as follows: (i) an increased stability of the system and the possibility to arrange spatially well-structured, nanoscopic devices and (ii) a distinctive photoresponse in zeolitic media. Because one property of many of catenanes and rotaxanes is to be photochemically active, our study on the photochemistry of the CT complexes based on cyclophane $\mathbf{2}^{4+}$ becomes relevant to demonstrate that these type of supramolecular assemblies will exhibit different photoresponses upon imprisonment within zeolites. For instance, undesired back electron transfer occurring in the subnanosecond time scale claimed[1] as responsible for the lack of operation of supramolecular motors and machinery could be slowed by encapsulation of such devices in appropriate aluminosilicates.

Experimental Section

Diffuse reflectance UV−vis spectra were recorded with a Shimadzu UV-2101/3101 PC scanning spectrophotometer adapted with an integrating sphere and using $BaSO_4$ as reference. IR spectra of self-supported compressed pellets (10 mg) were carried out in a greaseless IR quartz cell fitted with CaF_2 windows using a Nicolet 710 FT-IR spectrophotometer. The IR spectra were recorded at room temperature after outgassing under reduced pressure (10^{-2} Pa) at increasing temperatures for periods of 1 h. Solid-state ^{13}C CP NMR spectra were acquired on a Brucker ASX-200 solid-state NMR spectrometer operating at 50.3 MHz for ^{13}C. The cross polarization contact times were set to 1 ms and a 2 s relaxation delay was used. The samples were spun at 4500 Hz.

Laser flash photolysis experiments were carried out using the fourth (266 nm, ≤10 mJ × pulse^{-1}), third (355 nm, ≤20 mJ × pulse^{-1}) and the second (532 nm, ∼20 mJ × pulse^{-1}) harmonic of a Surelite Nd:YAG laser for excitation (pulse ≤10 ns). The signal from the monochromator/photomultiplier detection system were capture by a Tektronix 2440 digitizer and transferred to a Power PC Macintosh computer that controlled the experiment and provided suitable processing and data storage capabilities. Fundamentals[33,34] and details[35] of similar time-resolved diffuse-reflectance laser setup has been published elsewhere. Molecular modeling was performed on a Silicon graphics workstation using the Insight II program packages.

Compounds 1,1′-[1,4-phenylenebis(methylene)]bis-4,4′-bipyridinium bis(hexafluorophosphate), $(\mathbf{1}^{2+}(\mathbf{PF_6})_2)$, and cyclobis-(N,N′-paraquat-*p*-phenylene) tetrakis(hexafluorophosphate), $(\mathbf{2}^{4+}$-

$(PF_6)_4$), were prepared from 1,4-bis(bromomethylbenzene) and 4,4′-bipyridine followed by ion exchange according to the procedure reported in the literature[3].

1,1′-[1,4-Phenylenebis(methylene)]bis-4,4′-bipyridinium-Y (1^{2+}@Y). 1^{2+}-to-Na^+ ion exchange was carried out by stirring at room temperature for 24 h a suspension of the zeolite Y in its Na^+ form (1 g) in an aqueous solution of $\mathbf{1}^{2+}Br_2$ (0.3 g). After exchange the solid was filtered and dried. The final $\mathbf{1}^{2+}$ content was measured by thermogravimetry (C,N) (Neztch thermobalance operating under air stream using Kaolin as standard) and the percentage of ion exchange was determined to be $((\mathbf{1}^{2+})_{0.94}Na_{51}Si_{139}O_{384})$. The solid was analyzed by diffuse reflectance UV−Vis, FT-IR and MAS ^{13}C NMR.

Cyclobis-(N,N′-paraquat-*p*-phenylen)-Y (2^{4+}@Y). A solution of 1,4-bis(bromomethyl)benzene (0.19 g) in CH_2Cl_2 (30 mL) was added to the partially exchanged $\mathbf{1}^{2+}$**@Y** (3 g) previously dehydrated by heating it in an oven at 110 °C for 5 h. The suspension was stirred at reflux temperature for 24 h. More 1,4-bis(bromomethylbenzene) (0.078 g) was added and the reaction mixture was refluxed for an additional 40 h. Then the solid was filtered and submitted to exhaustive solid−liquid extraction using a micro-Soxhlet equipment and CH_2Cl_2 as the solvent. The extracted solid was analyzed by diffuse reflectance UV−Vis, FT-IR and MAS ^{13}C NMR.

CT Complexes of 1^{2+}@Y and 2^{4+}@Y with 1,4-dimethoxybenzene (DMB). $\mathbf{1}^{2+}$@Y and $\mathbf{2}^{4+}$@Y were dehydrated heating at 200 °C under reduced pressure (0.10 Torr) for 2 h. These dehydrated zeolites (0.1 g) were added to a solution of **DMB** (0.04 and 0.05 g respectively) in CH_2Cl_2 (25 mL). The suspension was stirred at room temperature for 24 h. Then, the solid was filtered off, washed with CH_2Cl_2 and dried (80 °C in vacuo, 1 h). The final content of **DMB** (1.5 mol per supercage) was determined by recording the UV−vis spectra of the DMB solutions before and after treatment with $\mathbf{1}^{2+}$@Y and $\mathbf{2}^{4+}$@Y and quantifying the decrease in concentration of **DMB**. These solids were analyzed by diffuse reflectance UV−vis.

Acknowledgment. Financial support by the Spanish DGES (H.G., Grant No. MAT2000/1768-CO2-01) and Canadian NSERC (J.C.S.) is gratefully acknowledged. H.G. and B.F. are indebted to the Spanish Ministry of Education for a fellowship to support his stay at Ottawa and a postgraduate scholarship, respectively.

References and Notes

(1) Balzani, V.; Credi, A.; Raymo, F. M.; Stoddart, J. F. *Angew. Chem., Int. Ed. Engl.* **2000**, *39*, 3348.

(2) Chia, S.; Cao, J.; Stoddart, J. F.; Zink, J. I. *Angew. Chem., Int. Ed. Engl.* **2001**, *40*, 2447.

(3) Anelli, P. L.; Ashton, P. R.; Ballardini, R.; Balzani, V.; Delgado, M.; Gandolfi, M. T.; Goodnow, T. T.; Kaifer, A. E.; Philp, D.; Pietraszkiewicz, M.; Prodi, L.; Reddington, M. V.; Slawin, A. M. Z.; Spencer, N.; Stoddart, J. F.; Vicent, C.; Williams, D. J. *J. Am. Chem. Soc.* **1992**, *114*, 193.

(4) Alvaro, M.; Chretien, M. N.; Ferrer, B.; Fornés, V.; García, H.; Scaiano, J. C. *Chem. Commun.* **2001**, 2106.

(5) Herron, N. *Inorg. Chem.* **1986**, *25*, 4714.

(6) Herron, N.; Stucky, G. D.; Tolman, C. A. *J. Chem. Soc., Chem. Commun.* **1986**, 1521.

(7) Scaiano, J. C.; García, H. *Acc. Chem. Res.* **1999**, *32*, 783.

(8) Khouw, C. B.; Davis, M. E. *ACS Symp. Ser.* **1993**, *517*, 206.

(9) Chen, N. Y.; Garwood, W. E.; Dwyer, F. G. *Shape Selective Catalysis in Industrial Applications*; Marcel Dekker: New York, 1989.

(10) Corma, A.; García, H. *J. Chem. Soc, Dalton Trans.* **2000**, 1381.

(11) Corma, A. *Chem. Rev.* **1995**, *95*, 559.

(12) Parry, E. P. *J. Catal.* **1963**, *2*, 371.

(13) Basila, M. R.; Kantner, T. R.; Rhee, K. H. *J. Phys. Chem.* **1964**, *68*, 3197.

(14) Hughes, T. R.; White, H. M. *J. Phys. Chem.* **1967**, *71*, 2192.

(15) Sankararaman, S.; Yoon, K. B.; Yabe, T.; Kochi, J. K. *J. Am. Chem. Soc.* **1991**, *113*, 1419.

(16) Yoon, K. B. *Chem. Rev.* **1993**, *93*, 321.

(17) Yoon, K. B.; Hubig, S. M.; Kochi, J. K. *J. Phys. Chem.* **1994**, *98*, 3865.

(18) Alvaro, M.; García, H.; García, S.; Marquez, F.; Scaiano, J. C. *J. Phys. Chem.* **1997**, *101*, 3043.

(19) Yoon, K. B.; Kochi, J. K. *J. Am. Chem. Soc.* **1989**, *111*, 1130.

(20) de Borba, E. B.; Amaral, C. L. C.; Politi, M. J.; Villalobos, R.; Baptista, M. S. *Langmuir* **2000**, *16*, 5900.

(21) Balzani, V.; Credi, A.; Armaroli, N. *NATO ASI Ser, Ser. C, Phys. Supramol. Chem.* **1996**, *485*, 163.

(22) Yoon, K. B.; Huh, T. J.; Corbin, D. R.; Kochi, J. K. *J. Phys. Chem.* **1993**, *97*, 6492.

(23) Hashimoto, S.; Hagiwara, N.; Asahi, T.; Masuhara, H. *Langmuir* **1999**, *15*, 3123.

(24) Hashimoto, S. *Tetrahedron* **2000**, *56*, 6957.

(25) Benniston, A. C.; Harriman, A. *NATO ASI Ser, Ser. C, Phys. Supramol. Chem.* **1996**, *485*, 179.

(26) Shida, T. *Electronic Absorption Spectra of Radical Ions*; Verlag Chemie: New York, 1988; Vol. 34.

(27) Soma, Y.; Soma, M.; Harada, I. *J. Phys. Chem.* **1984**, *88*, 3034.

(28) Soma, Y.; Soma, M.; Furukawa, Y.; Harada, I. *Clays Clay Miner.* **1987**, *35*, 53.

(29) Soma, Y.; Soma, M.; Harada, I. *J. Phys. Chem.* **1985**, *89*, 738.

(30) Fenn, D. B.; Mortland, M. M.; Pinnavaia, T. J. *Clays Clay Miner.* **1973**, *21*, 315.

(31) Alvaro, M.; Ferrer, B.; Fornes, V.; García, H., to be published.

(32) Cozens, F. L.; Régimbald, M.; García, H.; Scaiano, J. C. *J. Phys. Chem.* **1996**, *100*, 18 173−.

(33) Bohne, C.; Redmond, R. W.; Scaiano, J. C. In *Photochemistry in Organized and Constrained Media*; Ramamurthy, V., Ed.; VCH: New York, 1991; p Chapter 3, pp 79−132.

(34) Wilkinson, F.; Kelly, G. In *Handbook of Organic Photochemistry*; Scaiano, J. C., Ed.; CRC Press: Boca Raton, FL, 1989; Vol. 1, p 293.

(35) Kelly, G.; Willsher, C. J.; Wilkinson, F.; Netto-Ferreira, J. C.; Olea, A.; Weir, D.; Johnston, L. J.; Scaiano, J. C. *Can. J. Chem.* **1990**, *68*, 812.